Toroidal Confinement without Parallel Current: Interchange and Entropy Modes in a Warm Electron Dipole Plasma

Mike Mauel, Darren Garnier, Max Roberts, and Jay Kesner

Dept of Applied Physics and Applied Math, Columbia University, New York, NY USA

Plasma Science and Fusion Center, MIT, Cambridge, MA USA

2015 Sherwood Fusion Theory Conference
New York, NY
Poster Session II – March 17, 2015

1

Abstract

The axisymmetric magnetically levitated dipole guarantees omnigeneous particle drifts and is the only high-beta toroidal magnetic configuration that satisfies the Palumbo condition: the divergence of the perpendicular plasma current vanishes. The absence of parallel currents in a dipole-confined plasma is significant. Many tokamak instabilities, *e.g.* kink, tearing, ballooning, and drift modes, are not found in a plasma torus confined by a magnetic dipole [1]. Instead, interchange and entropy modes dominate plasma dynamics, and plasma profiles determine the level of turbulence. Turbulent transport causes centrally-peaked profiles and self-organization, as the plasma approaches a state of minimum entropy production [2,3]. These unique confinement and stability properties create a new paradigm of toroidal magnetic confinement and also link laboratory plasma confinement studies to the physics of planetary magnetospheres. Interchange mixing also appears in planetary magnetospheres driven by solar wind, but ionospheric currents regulate interchange motion in the magnetosphere [4]. The absence of field-aligned currents in the laboratory causes ion-inertial currents to set the global structure of low-frequency fluctuations. Measurements of electrostatic interchange and entropy modes in dipole-confined plasma show similar global structures when driven either by energetic trapped electrons, sonic plasma rotation, or warm electron pressure. Recent experiments with localized current-injection feedback and with pellet injection show variations with mode frequency and amplitude that are consistent with linear and quasilinear models of interchange and entropy modes computed from the flux-tube averaged gyrofluid equations [5].

1. Garnier, *et al.*, *Phys Plasmas*, **6**, 3431 (1999).
2. Kesner, *et al.*, *Phys Plasmas*, **18**, 050703 (2011).
3. Kobayashi, e*t al*, *Phys Rev Lett*, **105**, 235004 (2010).
4. Lyon, *Science*, **288**, 1987 (2000).
5. Ricci, *et al., Phys Plasmas*, **13**, 062102 (2006).

Two Laboratory Magnetospheres: Plasma Experiments without Field-Aligned Currents

LDX: High Beta Levitation & Turbulent Pinch

Ryan

24 Probes 1 m Radius

CTX: Polar Imaging, Current Injection. Rotation

Max
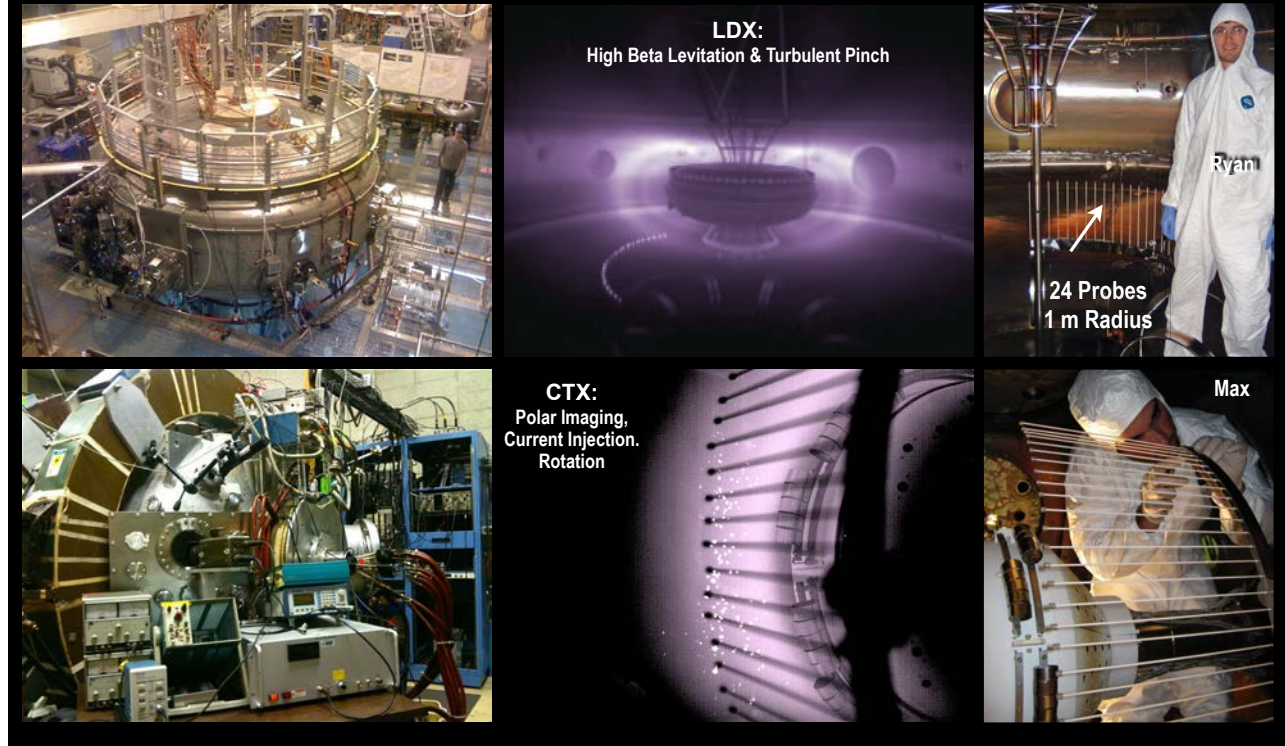
Flux-Tube Averaging Reveals Processes that Regulate Interchange Motion

$$\int \frac{ds}{B}\nabla_\perp \cdot \mathbf{J}_\perp = \begin{cases} 0 & \text{Closed, insulated, field lines} \\ 2(J_{||}/B)_{poles} & \text{Ionospheric current} \\ \sum_j I_j\,\delta(\psi-\psi_j)\delta(\phi-\phi_j) & \text{External circuits} \end{cases}$$

Steady MHD Convection in Space $\boxed{\hat{\mathbf{b}}\cdot\nabla\Phi = 0}$ Dynamic Drift-like Motion in Lab

Ion Inertial Currents

$$\mathbf{J}_\perp = \frac{\hat{\mathbf{b}}\times\nabla P}{B}\ \text{(space)}$$

$$\frac{2J_{||}}{B_{pole}} = \nabla_\perp P\cdot\hat{\mathbf{b}}\times\nabla_\perp\int\frac{ds}{B}$$

$$\nabla_\perp\cdot\Sigma_p\nabla_\perp\Phi \approx -J_{||}(\hat{\mathbf{b}}\cdot\hat{\mathbf{n}})\ \text{(poles)}$$

Ionospheric Conductivity

$$\mathbf{J}_\perp = \frac{\hat{\mathbf{b}}\times\nabla P}{B} - \frac{nM_i}{B^2}\nabla_\perp\frac{d\Phi}{dt}$$

$$\int\frac{ds}{B}\nabla_\perp\cdot\mathbf{J}_\perp = 0$$

$$\nabla_\perp\cdot\bar{\bar{\Sigma}}\cdot\nabla_\perp\frac{\partial\Phi}{\partial t} \approx -\nabla_\perp P\cdot\hat{\mathbf{b}}\times\nabla_\perp\int\frac{ds}{B}$$

Integrated Plasma Dielectric

Vasyliunas, "Mathematical Models of Magnetospheric Convection and Its Coupling to the Ionosphere," in *Particles and Fields in the Magnetosphere*, edited by B.M. McCormac (D. Reidel, Norwell, MA, 1970), pp. 60–71.

Planetary Magnetospheres

$$U_{con} \cong \frac{c^2}{8\pi \Sigma_p} \cdot \frac{\ell_{\parallel}}{L_{ps}} \cdot \ell n \left(\frac{p_{tot}^{(24)}}{p_{tot}^{(12)}} \right)$$
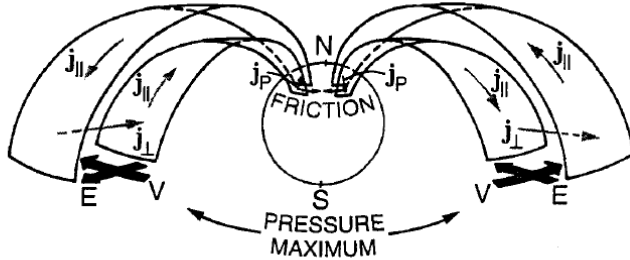
Figure 3. Dynamo forces, auroral current system, and resulting convection under frictional control by the ionosphere, after Boström (1964).
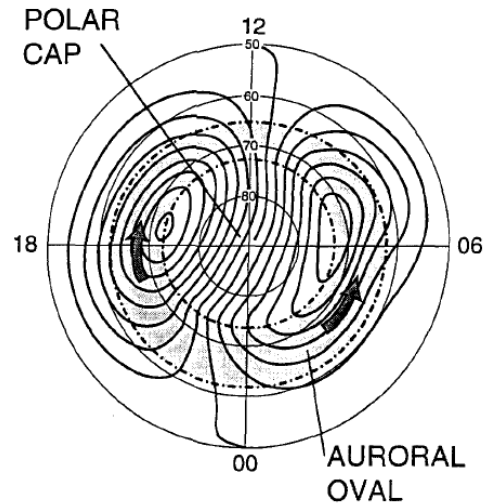
Figure 4. High-latitude plasma circulation system at times of an active magnetospheric dynamo (*e.g.* during substorms).

G. Haerendel, "Outstanding issues in understanding the dynamics of the inner plasma sheet and ring current during Storms and Substorms," *Advances in Space Research,* **25**, 2379 (2000).

5

Measured Ionospheric Currents
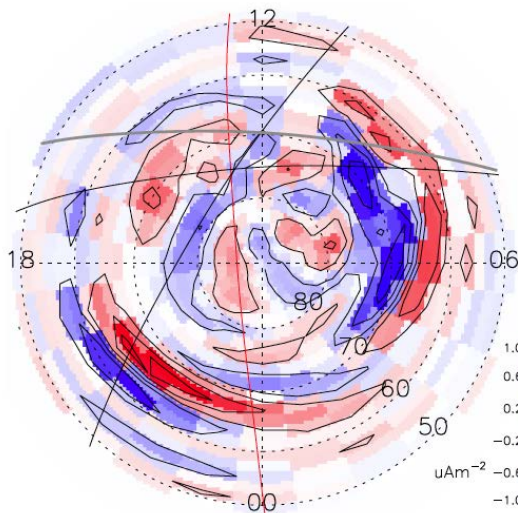
Fig. 6. Birkeland currents, $J_{\parallel}$ derived from the data in Fig. 4 according to Eq. (12) for 03:30–04:30 UT, 1 November, 2001. The DMSP and Oersted tracks are reproduced while the thicker, grey solid line from 06:00 to 18:00 MLT indicates the sunlight terminator boundary in the ionosphere.
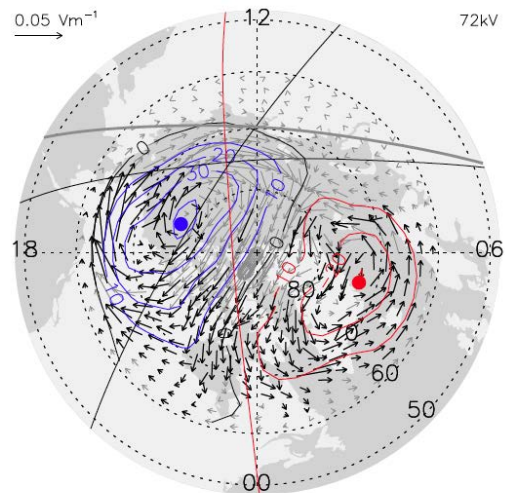
Fig. 7. Electric field vectors (rotated 90° counter clockwise) calculated from SuperDARN data averaged over 03:30–04:30 UT, 1 November, 2001. The electric potential contours, DMSP and Oersted tracks and the sunlight terminator are overlayed. The extremes in potential are located at the blue (-ve) and red (+ve) dots. The electric field vectors are bold at locations where radar returns were received.

Green, *et al.*, "Comparison of large-scale Birkeland currents determined from Iridium and SuperDARN data," *Annales Geophysicae* **24**, 941 (2006).

6

Measured Flute-Type Modes in CTX

Measured m = 1 Mode

Convective Structures are Dynamic

(φ ~ Stream function)
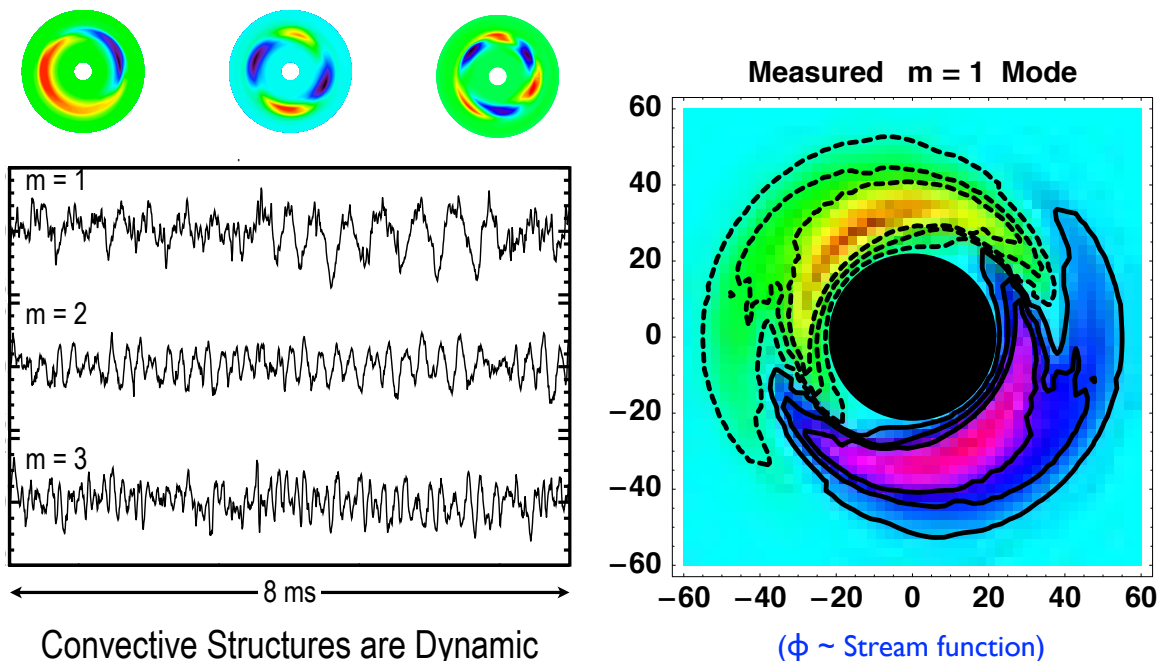
With $T_e \gg T_i$ (CTX and LDX) modes (usually) propagate in electron drift direction

---

Fast MHD Interchange in an Axisymmetric Magnetic Dipole

$$\mathbf{B} = \nabla\phi \times \nabla\psi \qquad \mathbf{B} \cdot \nabla = 0$$

- Electrostatic, low β

- $V_\perp = E \times B$

$$N(\varphi, \psi, t) = \int \frac{ds}{B} n, \ \text{(Particle Number)}$$

$$P(\varphi, \psi, t)\, U(\psi) = \int \frac{ds}{B} P, \ \text{(Isotropic pressure)}$$

- Adiabatic

$$\frac{\partial U}{\partial \psi} = \int \frac{ds}{B} \nabla\varphi \cdot \frac{2}{B}\hat{b} \times \kappa = -2\langle \kappa_\psi \rangle U$$

➡ Flux-tube averaged $\int \frac{ds}{B} \nabla_\perp \cdot \mathbf{J}_p = \frac{\partial U}{\partial \psi} \frac{\partial P}{\partial \varphi}$ (diamagnetic)

- 2D: (φ, ψ)

$$\int \frac{ds}{B} \nabla_\perp \cdot \mathbf{J}_i = -\frac{\partial}{\partial \psi}\left(N\, \Sigma_\psi \frac{\partial \dot{\Phi}}{\partial \psi} \right) - \frac{\partial}{\partial \varphi}\left(N\, \Sigma_\varphi \frac{\partial \dot{\Phi}}{\partial \varphi} \right)$$

$$\Sigma_\psi, \ \Sigma_\varphi = \frac{1}{N} \int \frac{ds}{B} \frac{n M_i}{B^2} |\nabla\psi|^2, \ \ldots, \ \text{(Polarization)}$$

- *Missing*: Entropy and drift-interchange modes

Linearized dimensionless MHD dynamics
Depends only upon ρ^* and profiles, h_n and h_g

- Equatorial radius, L_0

- Flux, $\psi_0 = B_0 L_0^2$ ($y \equiv \psi/\psi_0$)

- Gyroradius, $\rho^* = C_s / \omega_{ci} L_0 \ll 1$

- Potential, $M_i C_s^2/e$

- Pressure, $M_i C_s^2$

- Time, $1/(\omega_{ci} \rho^{*2})$

$$\boxed{\begin{aligned} h_n' &= \omega_n^* - \omega_d \\ h_g' &= \omega_p^* - \gamma\omega_d \end{aligned}}$$

$$\frac{\partial \tilde{N}}{\partial t} + \frac{dh_n}{dy}\frac{\partial \tilde{\Phi}}{\partial \varphi} = 0$$

$$\frac{\partial \tilde{P}}{\partial t} + y^{4\gamma}\frac{dh_g}{dy}\frac{\partial \tilde{\Phi}}{\partial \varphi} = 0$$

$$\rho_*^2 \frac{\partial}{\partial t}\left[\frac{\partial}{\partial y}\left(h_n\Sigma_\psi\frac{\partial\tilde{\Phi}}{\partial y}\right) + h_n\Sigma_\varphi\frac{\partial^2\tilde{\Phi}}{\partial\varphi^2}\right] + \frac{4}{y^5}\frac{\partial\tilde{P}}{\partial\varphi} = 0$$

$$\boxed{\text{When } h_n' \sim h_g' \sim 0, \text{ then } (\tilde{N}, \tilde{P}, \tilde{\Phi}) \to 0}$$

$$h_n(y) \equiv N(\psi)/N(\psi_0) \text{ and } h_g(y) \equiv P(\psi)U^\gamma/P(\psi_0)U(\psi_0)^\gamma$$

Local MHD Interchange Modes

$$\left\{\tilde{\Phi}(\psi,\varphi,t),\tilde{P},\tilde{N}\right\} = \sum_m \left\{\Phi_m(\psi), P_m(\psi), N_m(\psi)\right\} e^{-j(\omega_m t - m\varphi)}$$

m = 1, γ = 0.31/ρ*   m = 4, γ = 0.34/ρ*
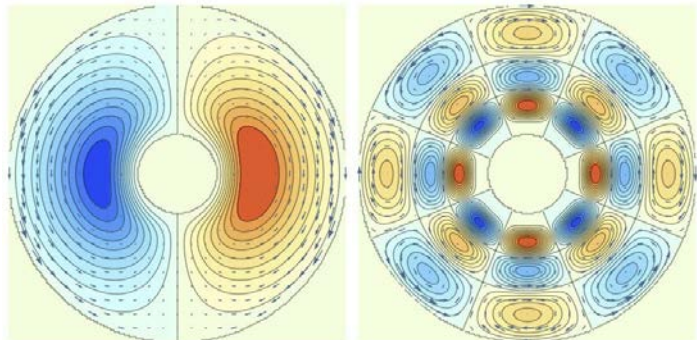
Example Eigenmodes: Unstable MHD Convection

$$\omega\tilde{N} - mh_n'\tilde{\Phi} = 0$$

$$\omega\tilde{P} - mh_g'\tilde{\Phi} = 0$$

$$\rho_*^2\omega\, m_\perp^2 \Sigma_\varphi\tilde{\Phi} + 4m\tilde{P} = 0$$

$$\omega = \pm\frac{2.5}{\rho^*}\frac{m}{m_\perp}\sqrt{-h_g'} \begin{cases} \omega_p^* > \gamma\omega_d, & \text{unstable} \\ \omega_p^* < \gamma\omega_d, & \text{stable} \end{cases}$$

$$\omega \propto \omega_{ci}\rho^*$$

Adding magnetic drift physics uncovers Entropy and Drift-Interchange Modes

- Near marginal stability, diamagnetic flows and magnetic drifts modify interchange dynamics in a significant and fundamental way…

- Flute-type entropy modes become unstable unless η ~ 2/3

- Density and pressure drift perturbations exist even for stationary profiles (*i.e. h'_n ~ h'_g ~ 0*)

- Entropy and drift-interchange instabilities propagate toroidally

- Bounce-averaged drift-kinetics applies (*relatively simple dynamics*)

- See…

  ‣ Kesner, *Phys Plasmas*, **7**, 3887 (2000)

  ‣ Beer and Hammett, *Phys Plasmas,* **3**, 4018 (1996).

  ‣ Ricci, Rogers, Dorland, and Barnes, *Phys Plasmas* **13**, 062102 (2006)

  ‣ Kobayashi, Rogers, and Dorland, *Phys Rev Lett,* **105**, 235004 (2010)

Entropy & Drift-Interchange Modes

(For CTX and LDX with $T_e \gg T_i$)

ω_{de} flow → ω_de flow

Collisionless heat flux due to Electron magnetic drift

$$\frac{\partial \tilde{N}}{\partial t} + \frac{dh_n}{dy}\frac{\partial \tilde{\Phi}}{\partial \varphi} + \frac{4}{y^5}\frac{\partial \tilde{P}_e}{\partial \varphi} = 0$$

$$\frac{\partial \tilde{P}_e}{\partial t} + y^{4\gamma}\frac{dh_g}{dy}\frac{\partial \tilde{\Phi}}{\partial \varphi} + \gamma\frac{4}{y^5}\left(\frac{y^{4\gamma}h_g}{h_n}\right)\left[2\frac{\partial \tilde{P}_e}{\partial \varphi} - \left(\frac{y^{4\gamma}h_g}{h_n}\right)\frac{\partial \tilde{N}}{\partial \varphi}\right] = 0$$

$$\rho_*^2\left(\frac{\partial}{\partial t} + \nu_i\right)\left[\frac{\partial}{\partial y}\left(h_n\Sigma_\psi\frac{\partial \tilde{\Phi}}{\partial y}\right) + h_n\Sigma_\varphi\frac{\partial^2 \tilde{\Phi}}{\partial \varphi^2}\right] + \frac{4}{y^5}\frac{\partial \tilde{P}_e}{\partial \varphi} = 0$$

ion-neutral damping

Local Entropy Drift-Interchange Modes

$$\omega \tilde{N} - m h'_n \tilde{\Phi} - 4m \tilde{P}_e = 0$$

$$\omega \tilde{P}_e - m h'_g \tilde{\Phi} - 4\gamma m (2\tilde{P}_e - \tilde{N}) = 0$$

$$\rho_*^2 (\omega + i\nu_i) m_\perp^2 \Sigma_\varphi \tilde{\Phi} + 4m \tilde{P}_e = 0$$

Interchange Stability ($m_\perp = 1$)   Interchange Stability ($m_\perp = 3$)

$\omega \sim \omega_{de}$
$\omega \sim -\omega_{de}$
Interchange $\omega_p^* > \gamma\omega_d$
Entropy $\eta < 2/3$
Entropy $\eta > 2/3$

$$\eta = \frac{h'_g + \gamma\omega_d}{h'_n + \omega_d} - 1$$

stable   stable

m = 1 with $\rho^* = 1/25$
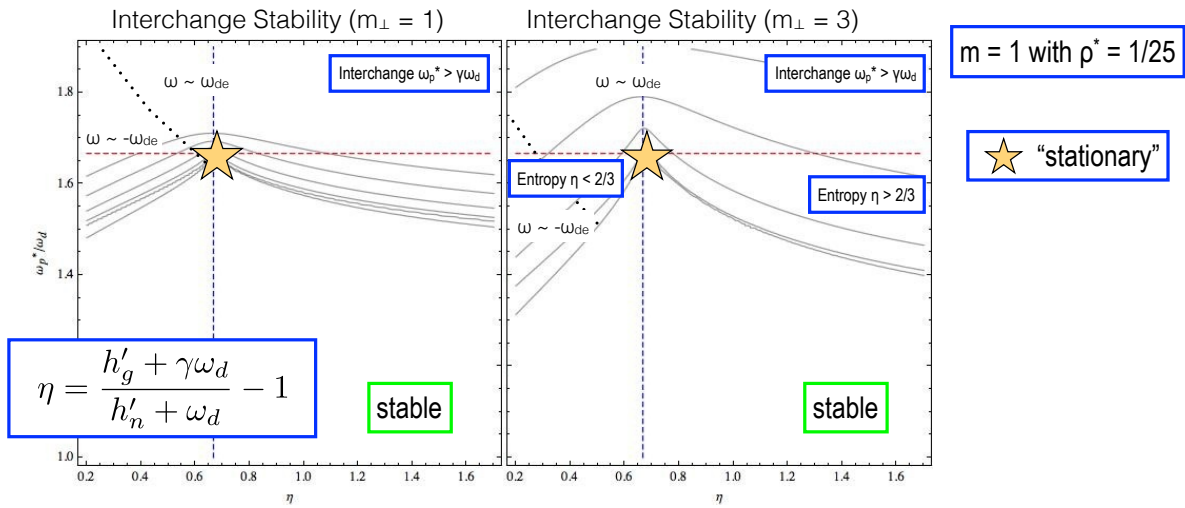
⭐ "stationary"

13

Comparing Low-Frequency Interchange-Drift Stability

(expressed with the usual tokamak normalized gradients)

$k_{\parallel} \neq 0$ $k_{\parallel} = 0$

Tokamak Stability   **Dipole Stability**

X. Garbet / C. R. Physique 7 (2006) 573–583   *J. Kesner, Phys Plasmas 7, 3837 (2000)*
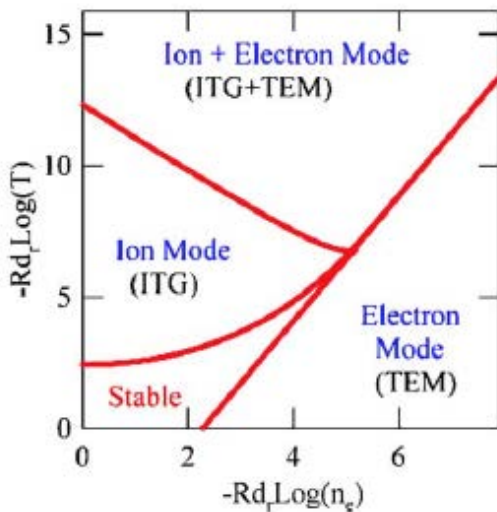
Ion + Electron Mode (ITG+TEM)
Ion Mode (ITG)
Electron Mode (TEM)
Stable
$-Rd_r Log(T)$
$-Rd_r Log(n_e)$

MHD Interchange Unstable
Stable
Entropy Mode
$-L\,d_l\,Log(T)$
$-L\,d_l\,Log(n)$

Dipole β ~ 1 Equilibrium
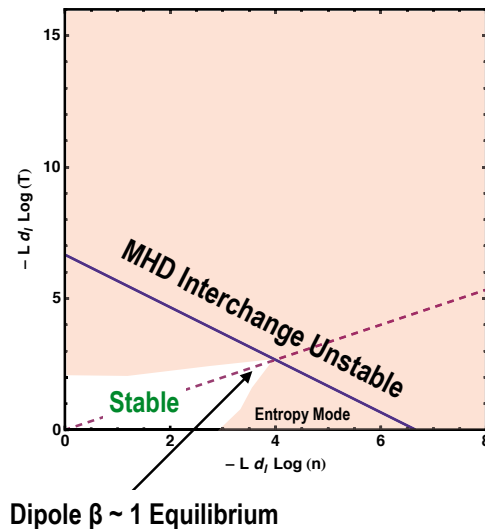
14

Stationary Drift Waves in a Dipole with Warm Electrons

When $h'_n \sim h'_g \sim 0$, then two stable drift waves and a damped convective cell.

$$\omega_m = i\nu_i \qquad\qquad \text{with } \tilde{N} \sim \tilde{P}_e \sim 0$$

$$\omega_m = m\omega_d \left(\gamma + \sqrt{\gamma(\gamma-1)}\right) \qquad \text{"fast" drift wave}$$

$$\omega_m = m\omega_d \left(\gamma - \sqrt{\gamma(\gamma-1)}\right) \qquad \text{"slow" drift wave}$$

"Slow" and "fast" drift waves correspond to flux tubes with locally "cooler" or "warmer" electrons relative to average, N/P_e.

When $h'_g \sim 0$, then the "fast" drift mode becomes an unstable **entropy mode** when $h'_n > 0.54 m_\perp^2 \rho_*^2$ (*i.e.* $\eta > 2/3$) and the "slow" drift mode becomes unstable whenever $h'_n < -4.8 m_\perp^2 \rho_*^2$ (*i.e.* $\eta < 2/3$) .

Profiles in CTX and LDX
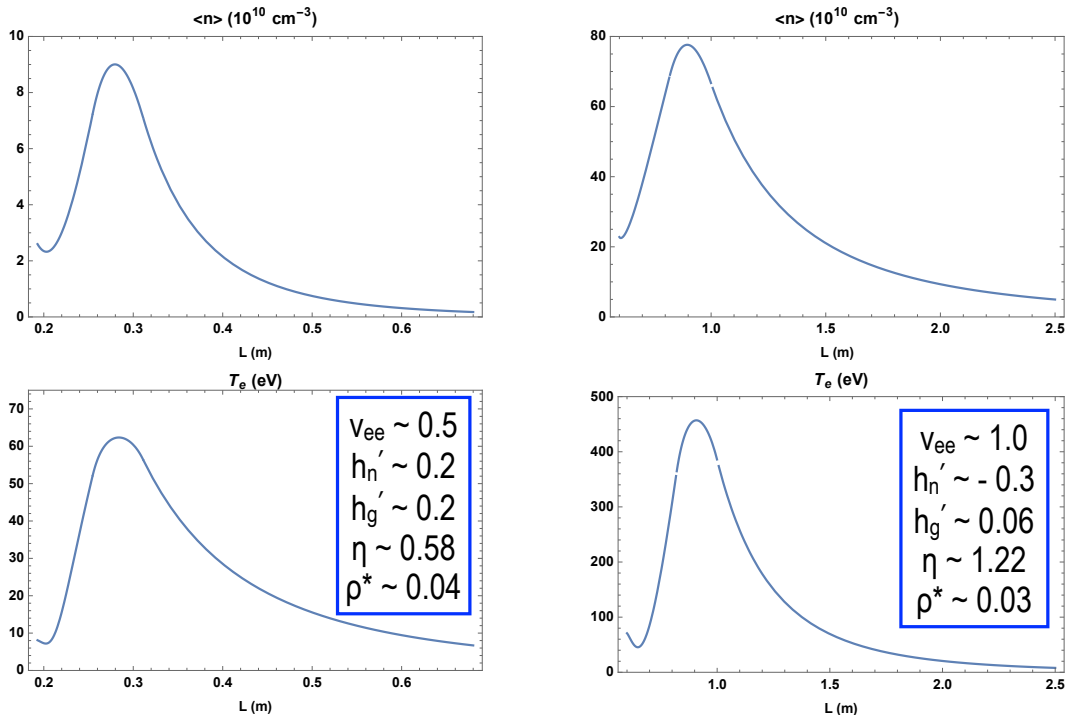
CTX and LDX have similar low-frequency flute-type dynamics

Example Drift-Interchange Eigenmodes

Φ (m = 1)   N (m = 1)   P (m = 1)

$(\omega_r, \gamma) = (1.6, 2.5)$
$\omega_r/2\pi = 3$ kHz

Φ (m = 6)   N (m = 6)   P (m = 6)

$(\omega_r, \gamma) = (6.5, 3.7)$
$\omega_r/2\pi = 12$ kHz
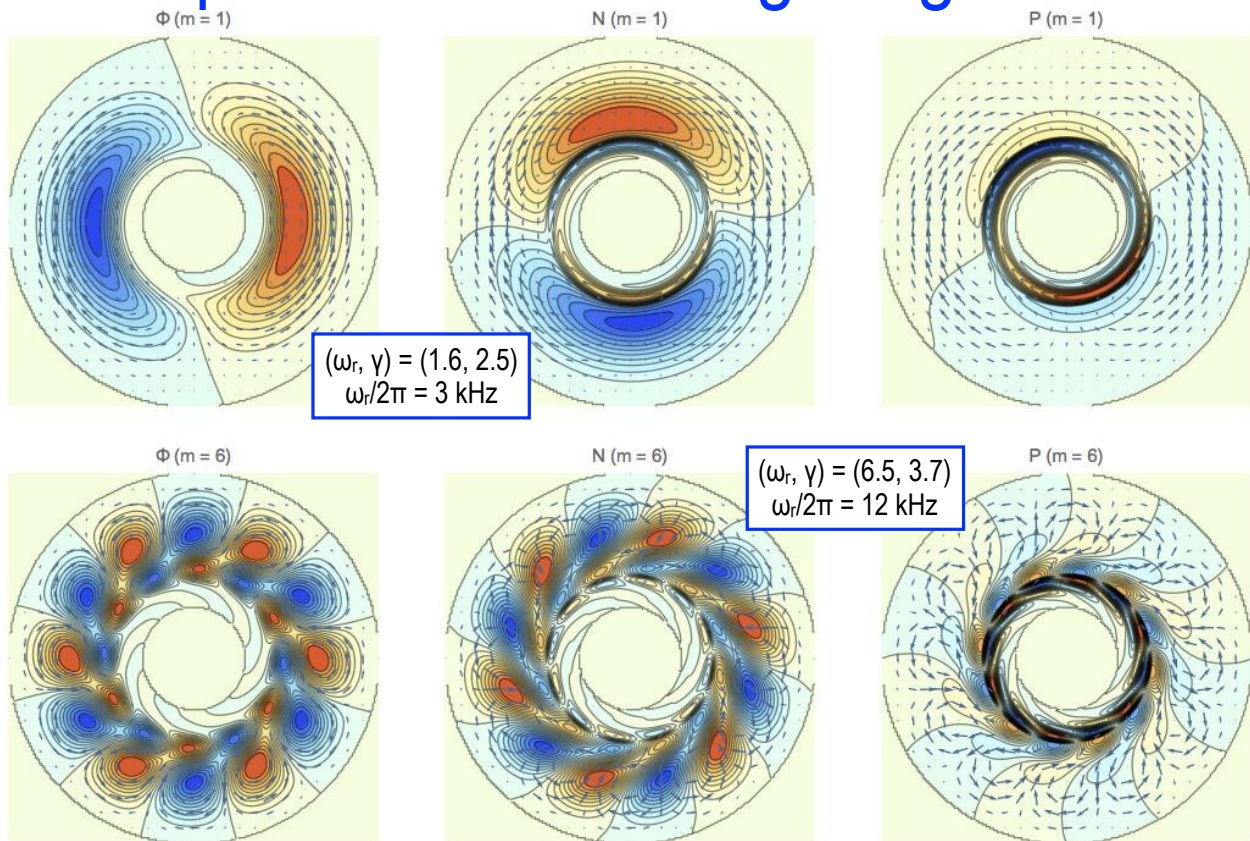
17

Entropy Mode Structure and Frequency Depends upon η

Φ (m = 1)   N (m = 1)   P (m = 1)

$h_g' = -0.03$

η ~ 0.37
$(\omega_r, \gamma) = (0.01, 2.6)$
$\omega_r/2\pi = 0.025$ kHz

Φ (m = 1)   N (m = 1)   P (m = 1)

η ~ 1.3
$(\omega_r, \gamma) = (5.1, 1.5)$
$\omega_r/2\pi = 10$ kHz
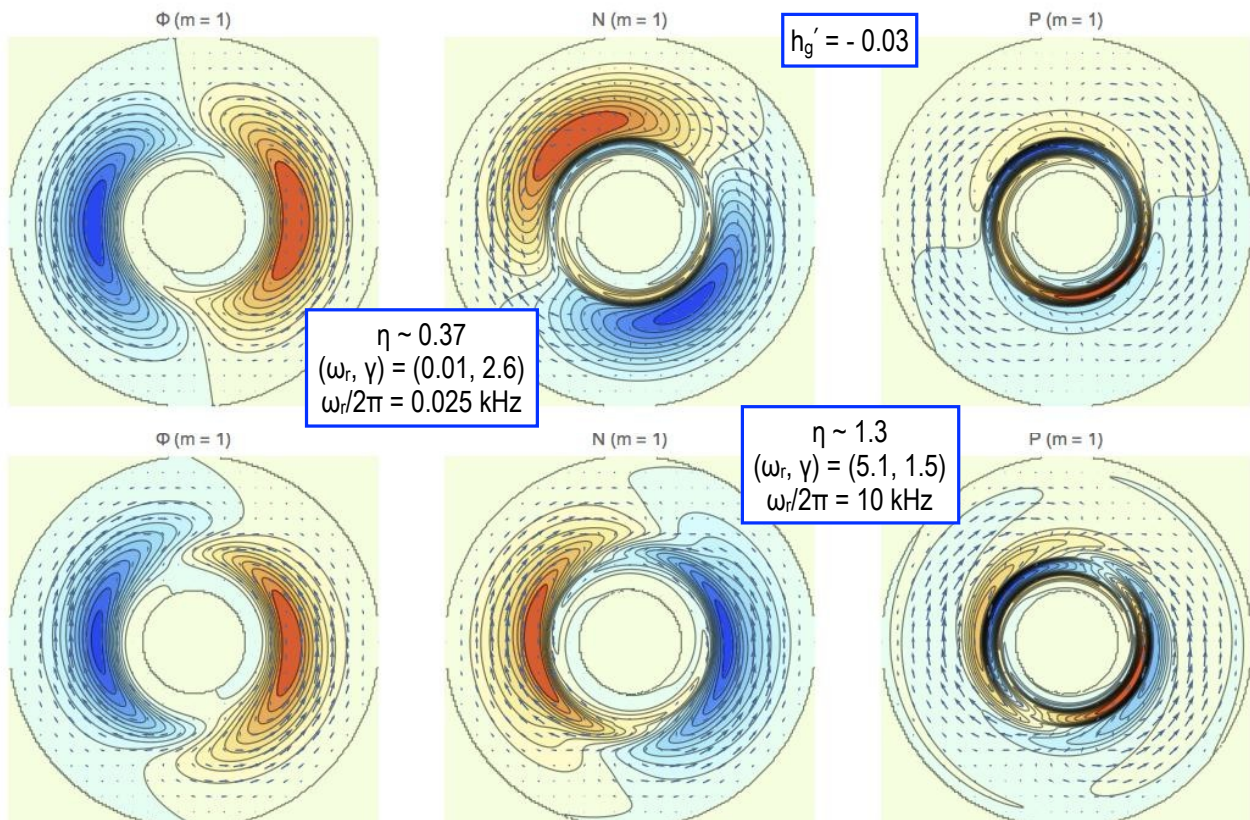
18

Particle Pinch in Gyrokinetic Simulations of Closed Field-Line Systems

Sumire Kobayashi[*] and Barrett N. Rogers[†]

Department of Physics and Astronomy, Dartmouth College, Hanover, New Hampshire 03755, USA

William Dorland[‡]

Department of Physics, University of Maryland, College Park, Maryland 20742, USA
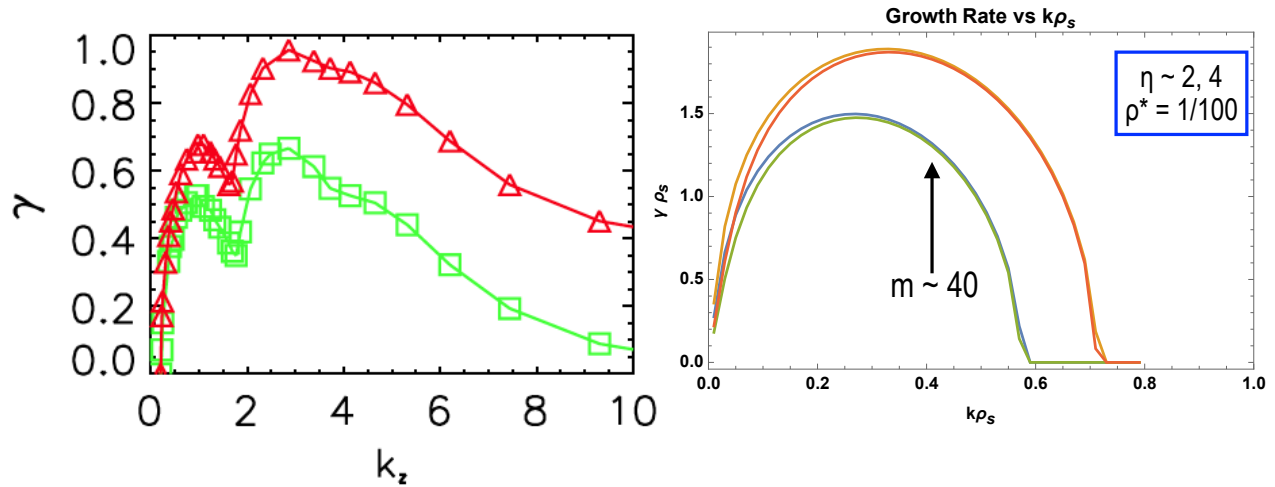
Peak growth rates for entropy mode have short wavelengths

19

Turbulent Intensity is Observed to Peak at Long Wavelengths (Inverse Mode-Mode Cascade)
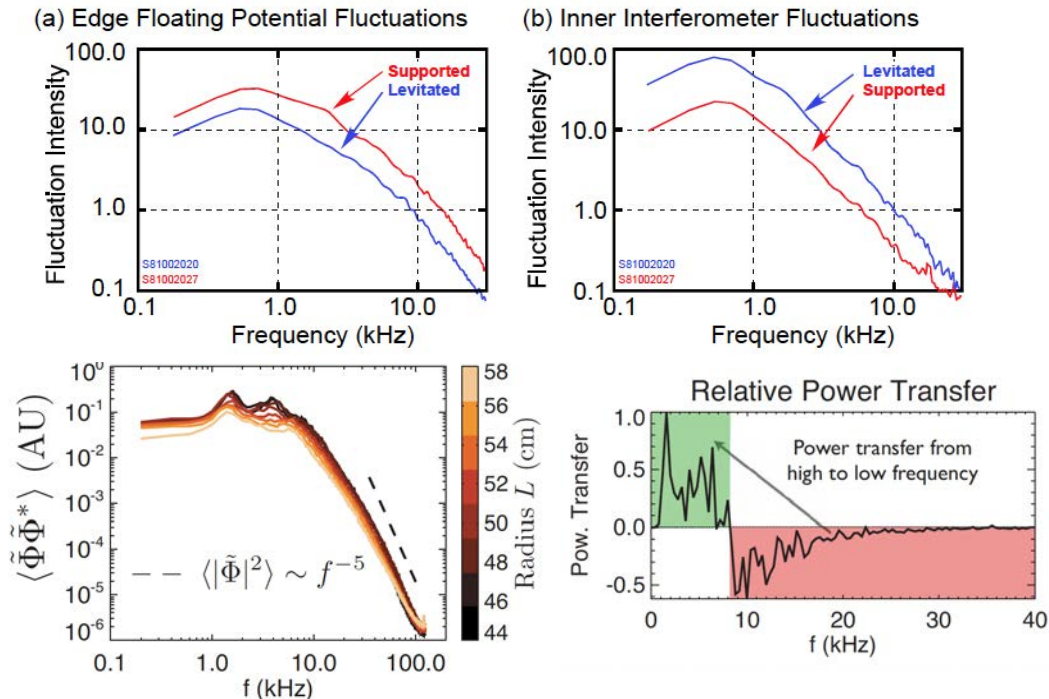
Grierson, M. Worstell, and M. Mauel, *Phys Plasmas* **16**, 055902 (2009).
Boxer, et al., *Nature Phys* **6**, 207 (2010).

20

Gyrofluid Quasilinear Theory

Quasilinear Resonance Functions for Interchange Transport

$$\frac{\partial \langle N \rangle}{\partial t} = -\frac{\partial}{\partial y} \sum_m \Re\{im\tilde{N}_m^* \tilde{\Phi}_m\}$$

$$\frac{\partial \langle G \rangle}{\partial t} = -\frac{\partial}{\partial y} \sum_m \Re\{im\tilde{G}_m^* \tilde{\Phi}_m\}$$
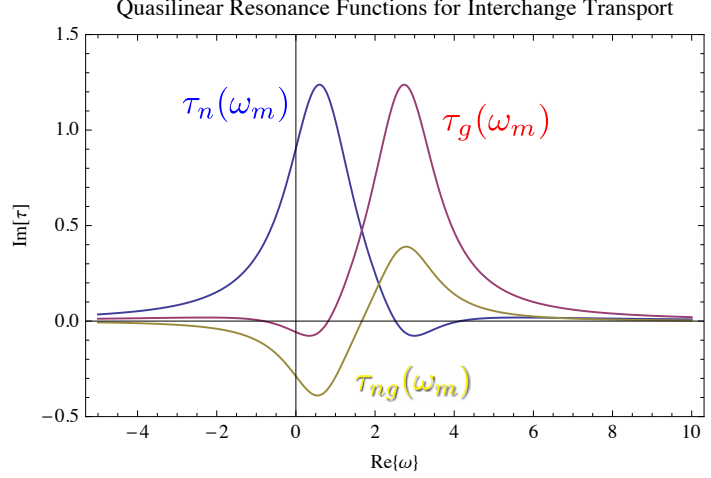
$$G \equiv PU^\gamma$$

Figure 2: Plot of the quaslinear resonance functions in Eqs. 28 and 29, $\Im\{\tau(\omega_m)\}$, for weakly growing interchange modes as a function of the real mode frequency, ω/ω_d. The quasilinear diffusion coefficients are the summation, over all modes, of the product of the mode intensity and the resonance functions. The blue curve is τ_n; the red curve is τ_g; and the gold curve is the cross-diffusion, τ_{ng}.

$$\tilde{N}_m = m\tilde{\Phi}_m \left(\tau_n(\omega_m)\frac{\partial \langle N \rangle}{\partial y} + \tau_{ng}(\omega_m)\frac{\partial \langle G \rangle}{\partial y} \right)$$

$$\tilde{G}_m = m\tilde{\Phi}_m \left(\tau_g(\omega_m)\frac{\partial \langle G \rangle}{\partial y} - \gamma\tau_{ng}(\omega_m)\frac{\partial \langle N \rangle}{\partial y} \right)$$

Quasilinear Theory Description of Particle and Pressure Pinches includes Cross-Gradient Flux

Using these linear forms for the perturbed density and pressure, the quasilinear transport equations are

$$\frac{\partial \langle N \rangle}{\partial t} = \frac{\partial}{\partial y} \sum_m m^2 |\Phi_m|^2 \left(\Im\{\tau_n(\omega_m)\}\frac{\partial \langle N \rangle}{\partial y} + \Im\{\tau_{ng}(\omega_m)\}\frac{\partial \langle G \rangle}{\partial y} \right) \quad (28)$$

$$\frac{\partial \langle G \rangle}{\partial t} = \frac{\partial}{\partial y} \sum_m m^2 |\Phi_m|^2 \left(\Im\{\tau_g(\omega_m)\}\frac{\partial \langle G \rangle}{\partial y} - \Im\{\tau_{ng}(\omega_m)\}\frac{\partial \langle N \rangle}{\partial y} \right). \quad (29)$$

Interchange transport fluxes have cross-terms that depend upon the frequency spectrum of the interchange turbulence. Peaked or hollow entropy density, $\partial \langle G \rangle/\partial y \neq 0$, can drive diffusion in flux-tube particle number, and peaked or hallow density, $\partial \langle N \rangle/\partial y \neq 0$, can drive diffusion in plasma pressure. The magnitude of the quasilinear fluxes depend upon the frequency spectrum. For a uniform turbulence spectrum, extending beyond a few times ω_d, the cross-diffusion fluxes vanish.

$$G \equiv PU^\gamma$$

Summary and Applications

- Global flux-tube averaged gryo-fluid description of flute-type instabilities describes drift-interchange and entropy modes

- Long wavelength eigenmodes and real frequencies like observations in CTX and LDX

  - Quasilinear theory describes up-gradient turbulent pinches

  - Linear theory can model local current-injection feedback (Roberts, *PoP 2015*)

  - Li pellet injection reduces $\eta \to 0$ and reverses toroidal propagation of fluctuations

- Need to include bounce-averaged drift-resonances, like Maslovsky, Levitt, and Mauel, *Phys Rev Lett* **90**, 185001 (2003) Beer and Hammett, *Phys Plasmas* **3**, 4018 (1996)

- Mode-mode and 2D interchange cascade may explain the discrepancy between observations dominated with low-*m* eigenmodes and linear high-*m* eigenmodes with large growth rates.

- Flux-tube averaging makes possible "whole-plasma" nonlinear turbulence simulations.

23

Local Regulation of Interchange Turbulence with Current-Collection Feedback

(Roberts, *Phys. Plasmas*, 2015)

Local Regulation of Interchange Turbulence with Current-Collection Feedback

(Roberts, *Phys. Plasmas*, 2015)

Measurement

Linear Theory

Electrostatic Potential Fluctuations

Perturbed Density

25

Pellet Fueling Drives η → 0

Li Pellet Injector

(1) Before

(2) Li Pellet

(3) ≥ x6 Density

26
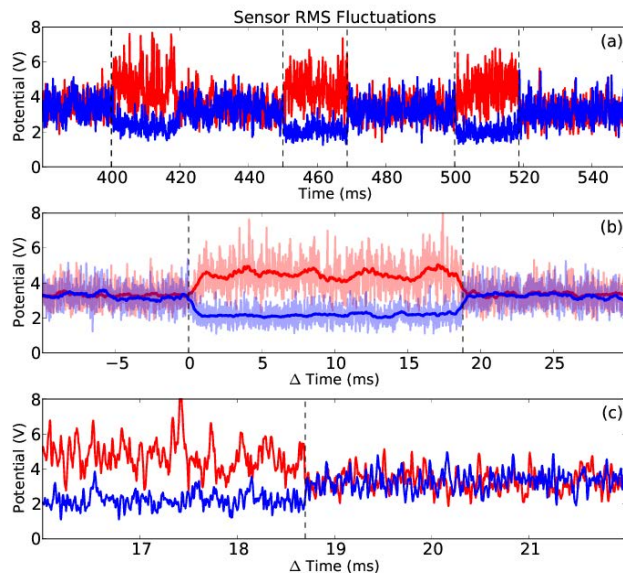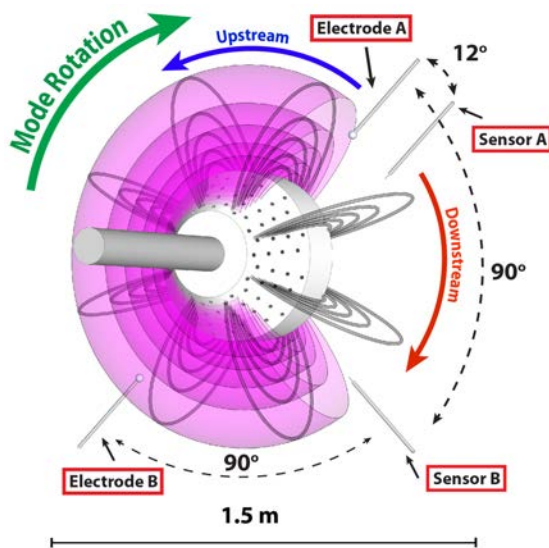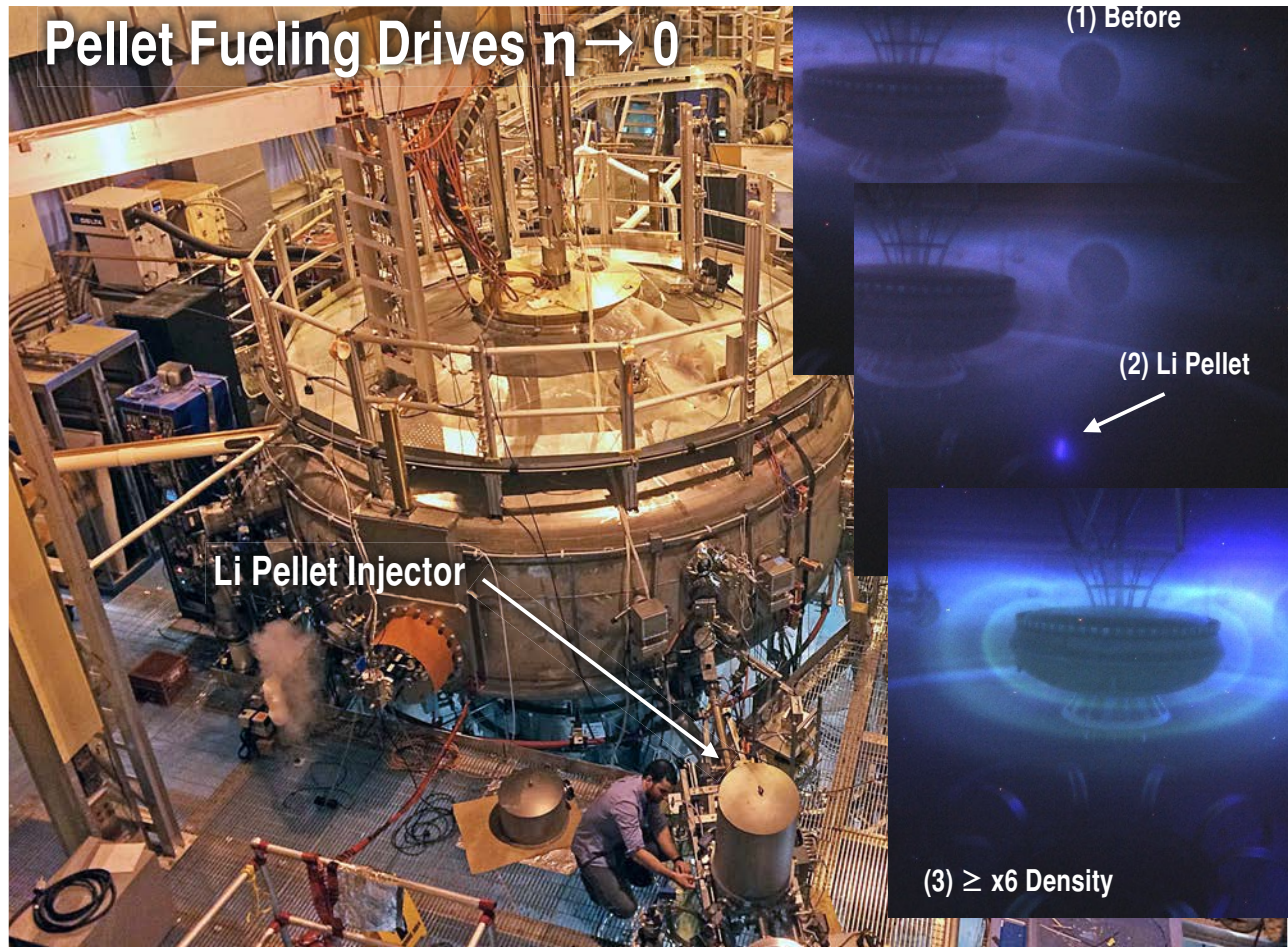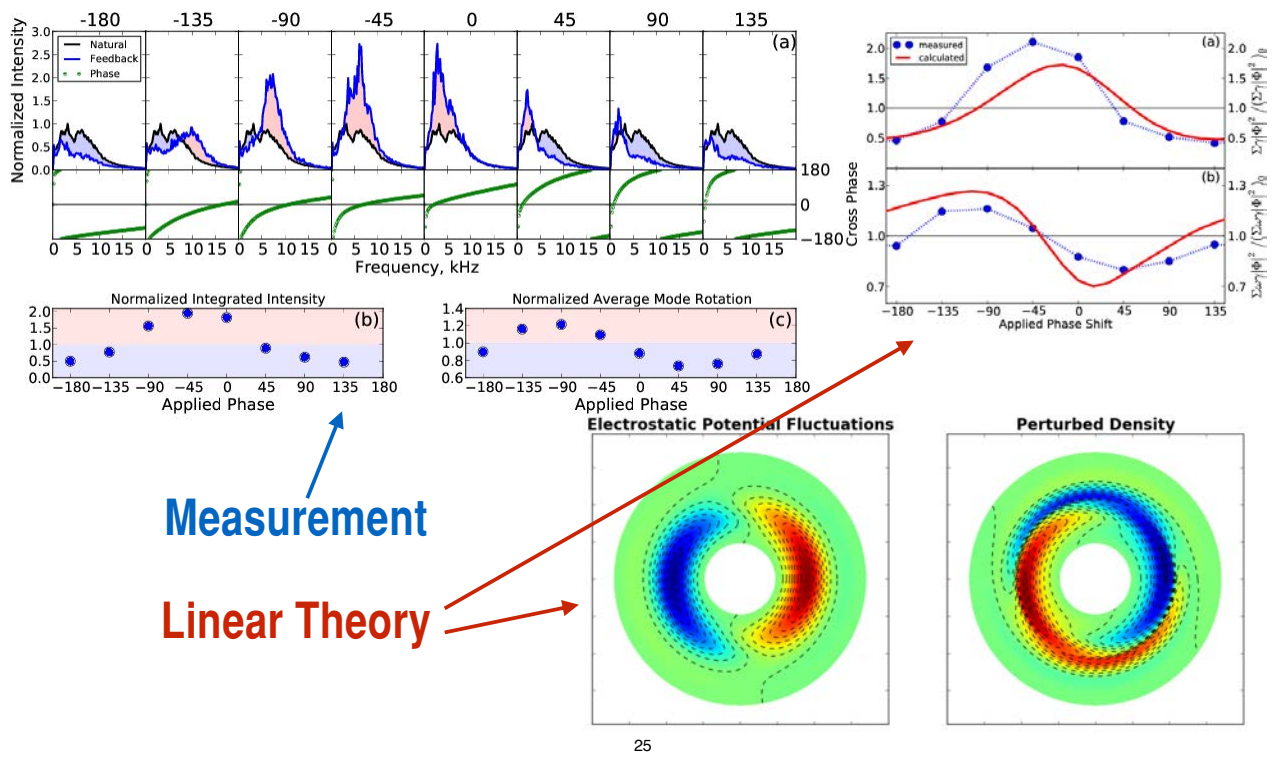
Li Pellet Injection Increases Density (x10) and Drives η → 0

(Garnier, DPP 2014 and to be submitted to PPCF, 2015)

- (**t₁**) Before Li pellet η > 2/3

  Entropy-Drift Interchange Mode rotates in **electron** direction

- (**t₂**) After Li pellet η ~ 0

  Entropy-Drift Interchange Mode rotates in **ion** direction

Probe Array Measures Mode Structure and Rotation
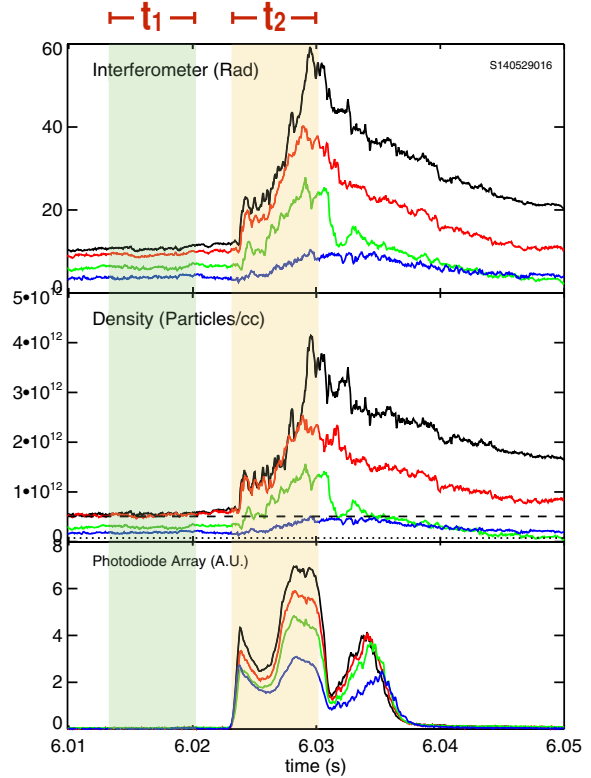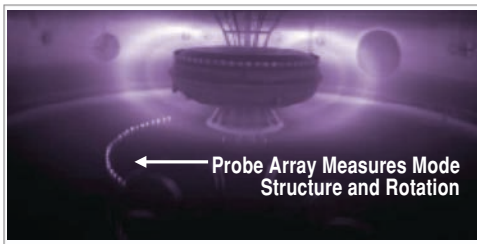
Li Pellet Injection Increases Density (x10) and Drives η → 0

(Garnier, DPP 2014 and to be submitted to PPCF, 2015)

(**t₁**) Before pellet η > 2/3
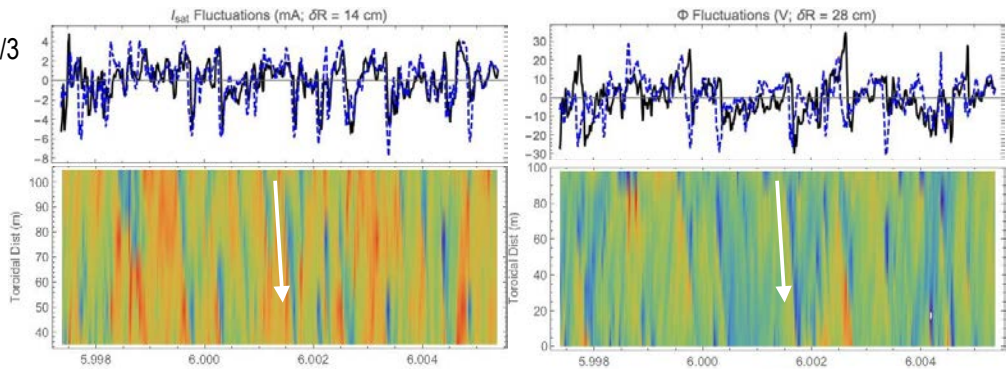
Entropy-Drift Interchange Mode rotates in **electron** direction

(**t₂**) After Li pellet η ~ 0

Entropy-Drift Interchange Mode rotates in **ion** direction
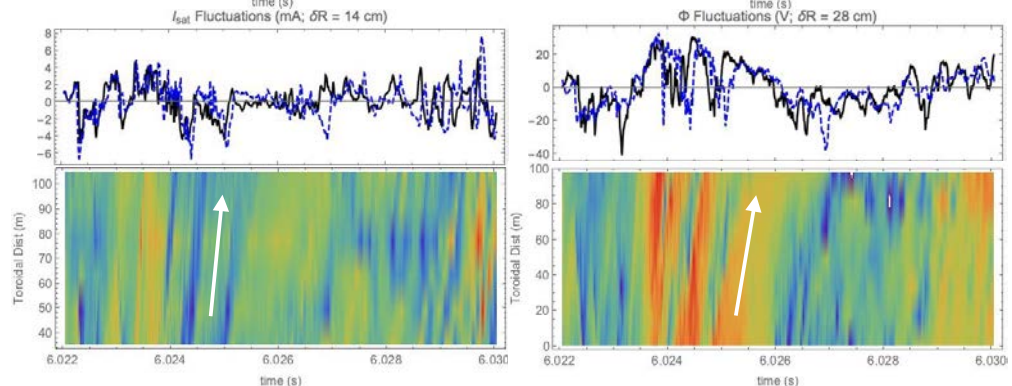
High β, Steady State, Self-Organized, Very-Large Plasma Torus
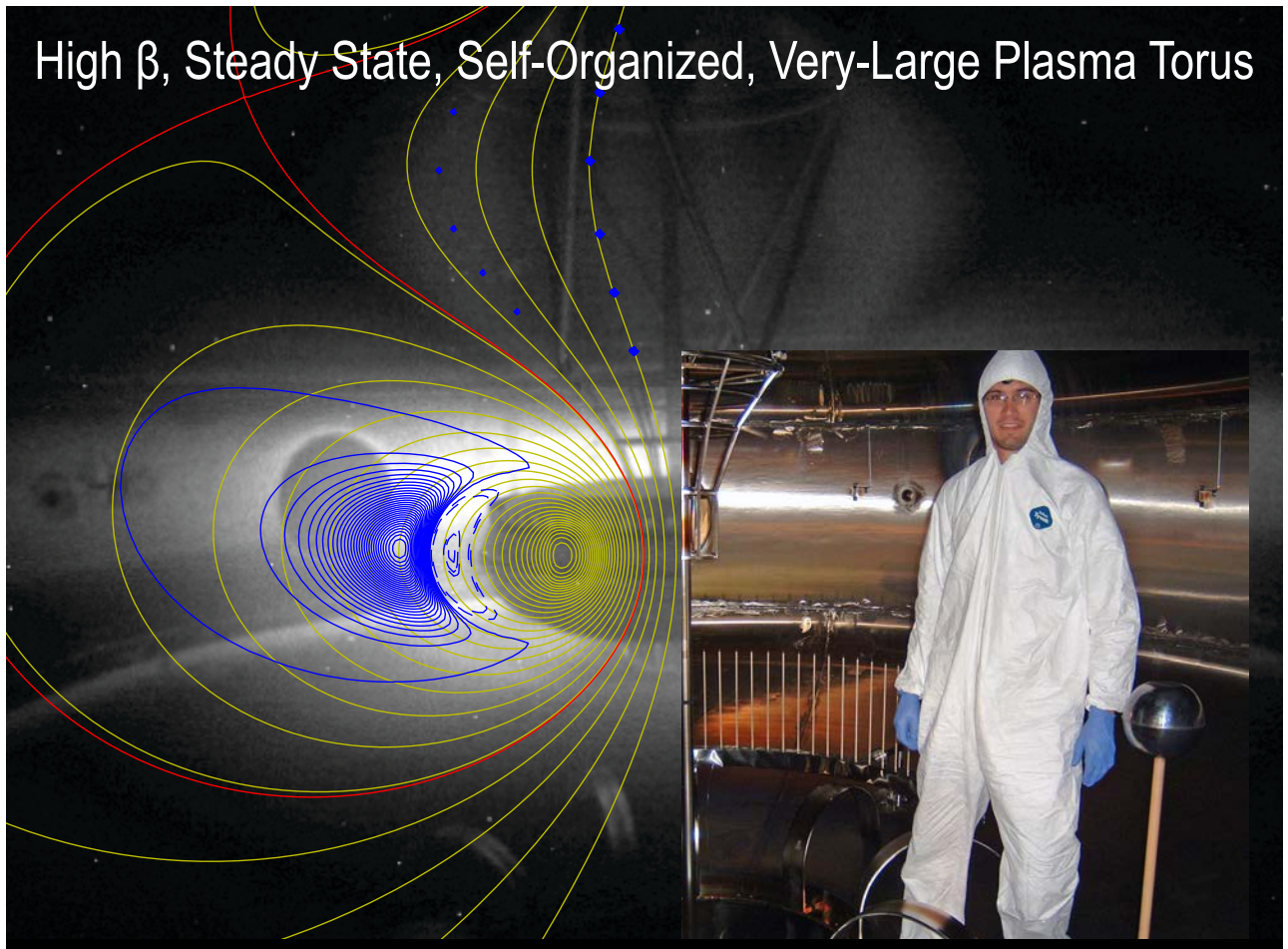
Toroidal Confinement without Toroidal Field may Speed Fusion Development Using Much Smaller Superconducting Coils
($Q_{DT} \sim 10$ Magnet Systems Compared at Same Scale)

Kesner, et al., *Nuclear Fusion* **44**, 193 (2004)

Toroidal and Poloidal Magnets

Small Levitated Magnet
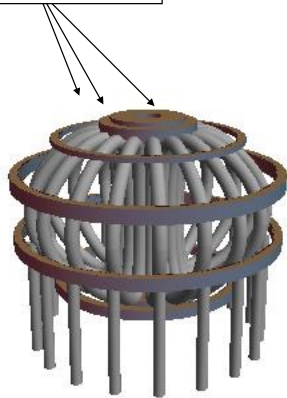
Plasma Volume = 837 m³

P_{fus} = 410 MW W_p = 1.1 GJ W_b = 51 GJ I_t = 164 MA

(a) Conventional Fusion Experiment (Gain = 10)
Gyro-Bohm Scaling

Plasma Volume = 42,000 m³

P_{fus} = 39 MW W_p = 0.06 GJ W_b = 1.6 GJ I_d = 25 MA

(b) Dipole Fusion Experiment (Gain = 10)
Bohm Scaling

30-fold size/energy reduction (!)